J Mater Sci (2010) 45:5883–5891
DOI 10.1007/s10853-010-4667-1

Hot working of Ti-17 titanium alloy with lamellar starting structure using 3-D processing maps

Kaixuan Wang · Weidong Zeng · Yongqing Zhao · Yunjin Lai · Yigang Zhou

Received: 11 March 2010 / Accepted: 26 May 2010 / Published online: 31 July 2010

Abstract Isothermal compression of Ti-17 titanium alloy with lamellar starting structure at the deformation temperatures ranging from 780 °C to 860 °C, the strain rates ranging from 0.001 to 10 s^{-1}, and the height reductions ranging from 15% to 75% with an interval 15% were carried out. Based on experimental results, 3-D processing maps including strain were developed and used to identify various microstructural mechanisms and distinguish the safe and unsafe domains. The processing maps exhibit two maximum power dissipation efficiency domains and dynamic globularization takes place in this two domains. The first domain occurs at 800–860 °C and at strain rates lower than 0.01 s^{-1}, and the second occurs at 780–800 °C and at strain rates lower than 0.01 s^{-1}. With the increasing of the strains, the values of maximum power dissipation efficiency in this two domains increase. One flow instability domain due to adiabatic shear bands and lamellar kinking occurs at strain rates higher than 0.487 s^{-1}, lower temperature, and higher strain above 0.2. The instability deformation region increases with increasing strain, strain rate, and decreasing temperature.

Introduction

Ti-17 (Ti–5Al–2Sn–2Zr–4Mo–4Cr) titanium alloy is a "beta-rich" two phase alloy, which is developed primarily for gas turbine engine components, such as disks for fan and compressor stages [1]. Recently, Ti-17 alloy has received increasing attention in China due to its potential for manufacturing dual-property blisk (composed of a disk and blades). It is known that the dual-property blisk should have a lamellar microstructure in disk section and equiaxed microstructure in the blades. For hot working of the dual-property blisk, the perform is usually pre-forged in β phase field to obtain a transformed microstructure consisting of acicular or lamellar morphology, and subsequent forging in $\alpha + \beta$ phase field to change the lamellar microstructure in the blade region to equiaxed or globularized microstructure. It is significant to investigate the effect of deformation parameters on the dynamic globularization of lamellar microstructure during hot working. In addition, the hot workability in $\alpha + \beta$ phase field is limited by the narrow range of forming temperature and the generation of various deformation defects such as micro-cracking and flow instability. Therefore, it is necessary to characterize hot deformation behavior and optimize hot working parameters in order to achieve microstructural control and successful forging.

Processing maps have been developed to optimize workability, control microstructures, and avoid defects for some titanium alloys [2–11]. Seshacharyulu et al. [3] investigated microstructural mechanisms during hot working of commercial grade Ti–6Al–4V with lamellar starting microstructures. Prasad et al. [5] reviewed the applications of the processing map based on dynamic materials model to characterize the deformation behavior including dynamic recrystallization (DRX), superplastic deformation, wedge cracking, adiabatic shear bands formation, and globularization of lamellar microstructure. Li et al. [7] identified various microstructural mechanisms and distinguished the safe and unsafe domains of hot working

K. Wang (✉) · W. Zeng · Y. Zhou
School of Materials Science and Engineering, Northwestern Polytechnical University, Xi'an 710072, China
e-mail: kxwang_nwpu@yahoo.cn

K. Wang · Y. Zhao · Y. Lai
Northwest Institute for Nonferrous Metal Research, Xi'an 710016, China

of Ti–6Al–3Mo–2Zr–0.3Si with lamellar $\alpha + \beta$ starting microstructures. Zhou et al. [9] investigated the globularization of lamellar structure in TC17 (viz. Ti-17) titanium alloy, but there was a flaw in analyzing the dynamic globularized mechanisms based on processing maps and the heat-treated microstructure, because the static globularization occurred during heat-treatment followed by hot deformation. However, the traditional processing maps do not involve the variation of strain, and the influence of strain on workability cannot be represented. Thus, for metals or titanium alloys characterized by strain softening, the strain is found to be a significant and non-negligible influential factor. 3-D processing maps including strain are developed and used to identify various microstructural mechanisms and distinguish the safe and unsafe domains. 3-D processing maps describe the variations of the efficiency of power dissipation and flow instability domains with strain rate, temperature, and strain, which deal with the sensitivity of the workability to strain at elevated temperature. Liu et al. [12] investigated the metal workability of magnesium alloy AZ31B characterized by strain softening using 3-D processing maps, and 3-D processing maps effectively describe the microstructural evolution mechanism and the flow instability domains under certain conditions but also provide optimum deformation temperature range and strain rate range.

In the present paper, the hot deformation behavior of Ti-17 alloy with a lamellar starting structure was examined by isothermal compressive tests in $\alpha + \beta$ phase field. 3-D processing maps including strain were constructed, which demonstrated the variation of power dissipation efficiency and flow instability domains at different temperatures, strain rates and strains. Subsequently, the processing maps were used to identify various microstructural mechanisms and safe and unsafe domains through microstructure observations. The optimum workability is designed by the processing maps.

Experimental procedures

The measured compositions (wt%) of Ti-17 titanium alloy used in this investigation were as follows: 5.02Al, 3.93Cr, 3.88Mo, 2.37Sn, 1.95Zr, 0.05Fe, 0.01C, 0.01N, 0.003H, 0.12O, and balance Ti. The beta transus temperature was determined via a series of heat treatments to be 905 °C. The microstructure with the starting material is shown in Fig. 1. The starting alloy has a lamellar microstructure with coarse prior β grains (400 μm grain size), 20–30 μm length, about 0.5 μm thick alpha lamellae. In addition, a random orientation of alpha lamellae is observed.

Isothermal compression of the Ti-17 titanium alloy at a constant strain rate was conducted on a Gleeble-1500 thermal simulation machine at deformation temperatures ranging from 780 °C to 860 °C with an interval of 20 °C and strain rates ranging from 0.001 s^{-1} to 10 s^{-1} at an interval of an order of magnitude. The specimens were heated and held 300 s at the deformation temperature prior to isothermal compression. The cylindrical specimens' ends were grooved for retention of the glass lubricants used during compression tests. The cylindrical specimens with 8 mm diameter and 12 mm height were axially pressed to ordered reduction and were quenched directly in water. Deformed specimens were axially sectioned parallel to the compression axis and the cut surface was prepared for metallographic examination using conventional techniques. The specimens for microstructural examinations were etched by the following solution: 12% HF, 18% HNO_3, and 70% H_2O. The microstructures of compressed specimens were directly observed by optical microscopy and scanning electros microscopy.

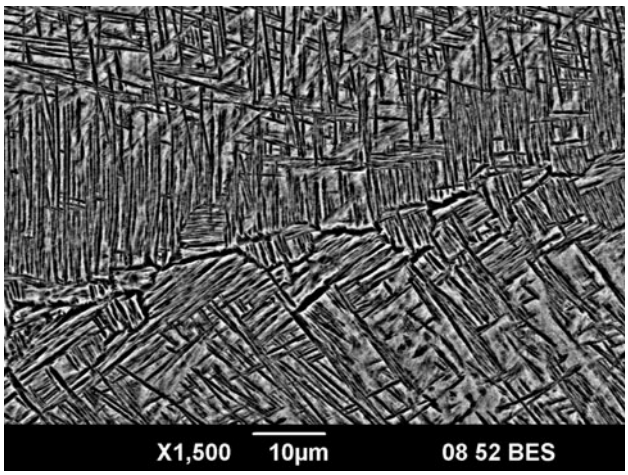

Fig. 1 SEM backscattered micrograph of Ti-17 alloy with lamellar starting structure

Approach of processing maps

The processing map was developed on the basis of the dynamic material model (DMM) [13–15]. According to DMM, the workpiece undergoing high temperature deformation can be considered as a nonlinear dissipater of the power. The instantaneous total power dissipated, P, may be written as follows:

$$P = \sigma\dot{\varepsilon} = \int_0^{\dot{\varepsilon}} \sigma \mathrm{d}\dot{\varepsilon} + \int_0^{\sigma} \dot{\varepsilon}\mathrm{d}\sigma = G + J \quad (1)$$

where σ is flow stress, $\dot{\varepsilon}$ is the strain rate. The first integral is defined as G content and represents the power dissipation due to plastic deformation, most of which is transformed into viscoplastic heat. The second integral is defined as J

co-content and is related to the power dissipation through metallurgical changes. The power partitioning between G and J is controlled by the constitutive flow behavior of the material, and it is given by the strain rate sensitivity (m) as follows:

$$m = \mathrm{d}J/\mathrm{d}G = (\dot{\varepsilon}\mathrm{d}\sigma)/(\sigma\mathrm{d}\dot{\varepsilon}) = (\partial(\log\,\sigma)/\partial(\log\,\dot{\varepsilon}))_{\varepsilon,\mathrm{T}} \approx \mathrm{d}\log\sigma/\mathrm{d}\log\dot{\varepsilon} \quad (2)$$

The dissipator co-content J can be written as

$$J = \sigma\dot{\varepsilon}m/(1+m) \quad (3)$$

By comparing the dissipation of the workpiece with that of an ideal linear dissipater, the efficiency of power dissipation (η)—a dimensionless parameter can be defined as

$$\eta = J/J_{\max} = 2m/(m+1) \quad (4)$$

The parameter η indicates the efficiency of the energy dissipation by microstructural evolution and determines the optimum conditions for thermomechanical processing. The variation of η with temperature and strain rate constitutes the power dissipation map.

A continuum criterion for the occurrence of flow instability is given by utilizing the extremum principles of irreversible thermodynamics as follows [16]:

$$\xi(\dot{\varepsilon}) = \partial\ln[m/(m+1)]/\partial\ln\,\dot{\varepsilon} + m < 0 \quad (5)$$

where $\xi(\dot{\varepsilon})$ is the instability parameter which varies with the deformation temperature and strain rate. Flow instability occurs when $\xi(\dot{\varepsilon})$ is negative. A processing map is obtained through being superimposed an instability map on a power dissipation map. Different domains in the power dissipation map implied the specific microstructural mechanisms. Domains implying specific microstructural mechanisms may be identified in the processing maps. Metal response to deformation depends upon the temperature, level and type of stress applied, strain rate, and other environmental factors [17–19]. For safe operation of any component under dynamic conditions, understanding the mechanism of plastic deformation and crack initiation is very important [19]. The "safe" mechanisms include dynamic recovery, DRX, and superplastic deformation, while the microstructural "damage" mechanisms include void formation, wedge cracking, intercrystalline cracking, and other types of cracking processes [5]. The optimum process parameters corresponding to the peak efficiency in safe domain, and the ranges of the processing parameters (widths of the domain in temperature and strain rate axes) may be obtained from the processing maps.

The following matters are important in the development of 3-D processing maps [12]: (1) at every fixed tested temperature and strain rates, the flow stress value at different strains must be extracted from flow stress–strain curves based on isothermal compression tests; (2) cubic spline interpolation is carried out to compute the flow stress values at no tested temperatures and strain rates, using the extracted data points as knots; (3) to compute the strain rate sensitivity, m, the logarithm relations of flow stress as a function of strain rate should also be fitted to third degree polynomial using least square method; (4) the value of efficiency of power dissipation (η) and the instability parameter $\xi(\dot{\varepsilon})$ can be obtained according to Eqs. 4 and 5; and (5) 3-D processing maps are plotted. The tasks 2–5 may be implemented using the software MATLAB 7.0.1.

Results

Stress–strain behavior

Selected flow stress–strain curves were obtained for two cases: one is at a deformation temperature of 820 °C and the strain rates ranging from 0.001 s^{-1} to 10 s^{-1}, and

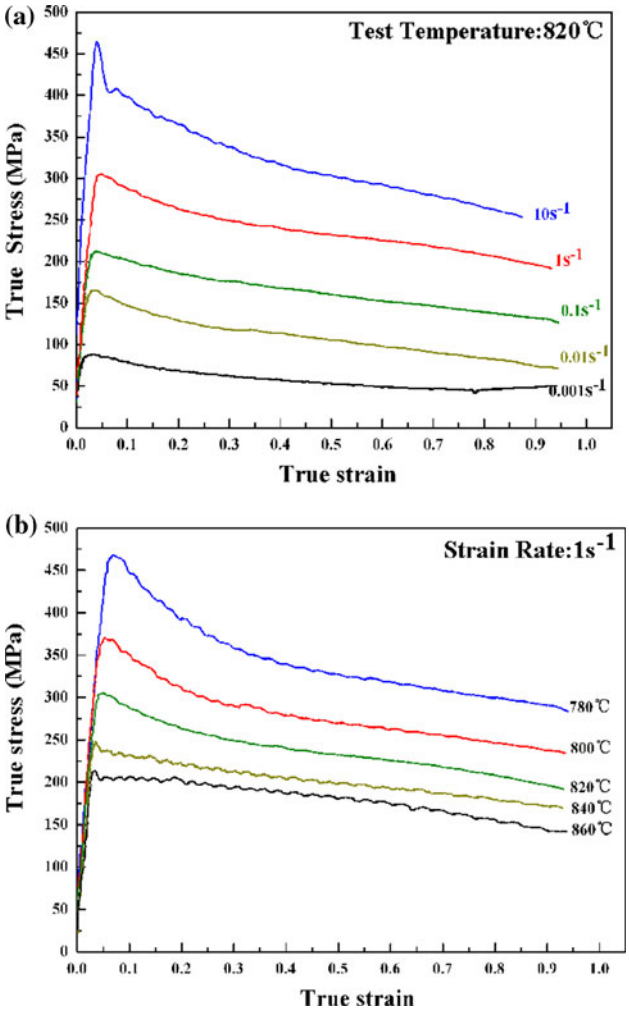

Fig. 2 Flow stress–strain curves in the isothermal compression of Ti-17 titanium alloy: **a** 820 °C and **b** 1 s^{-1}

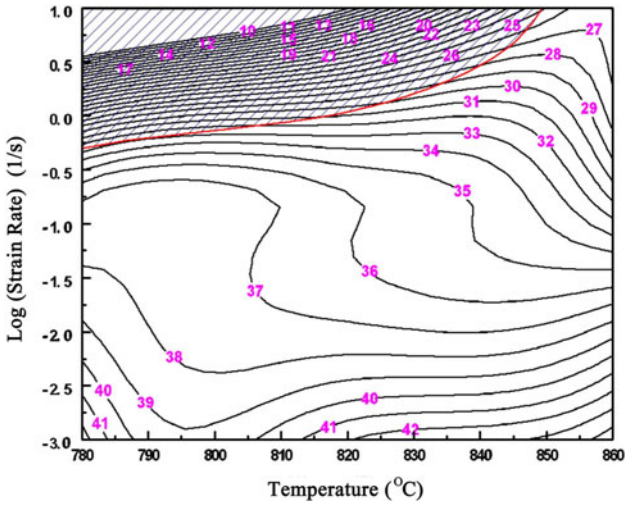

Fig. 3 Processing map of Ti-17 alloy at strain of 0.6

another is at a strain rate of 1 s^{-1} and deformation temperatures ranging from 780 °C to 860 °C presented in Fig. 2a, b. The flow stress–strain curves under other conditions may be obtained from our previous work [20]. The shape of stress–strain curves indicates some features helping to identify the mechanisms of hot deformation, although not in a conclusive fashion [3, 21]. Ti-17 alloy exhibits flow softening at all strain rates. In addition, the stress–strain curves of Ti-17 alloy display significant oscillatory flow at higher strain rates ($\geq$1 s^{-1}). Those broad oscillations may be induced by instable deformation [7]. It is difficult to determine the deformation mechanisms according to the shapes of the stress–strain curves, because the different microstructural mechanisms of hot deformation may result in similar stress–strain behavior [7]. Flow softening may indicate lamellar globularization, DRX, adiabatic heating, voids and cracks formation, etc. Steady state flow curve may indicate superplasticity or dynamic recovery. Therefore, the hot working behavior is further analyzed in the subsequent sections.

Processing maps of the Ti-17 alloy

The processing map of the Ti-17 alloy obtained at a strain of 0.6 is shown in Fig. 3. The contour numbers indicate the efficiency of power dissipation (η) and the shaded areas represent the flow instability region. The processing map exhibits two maximum power dissipation efficiency

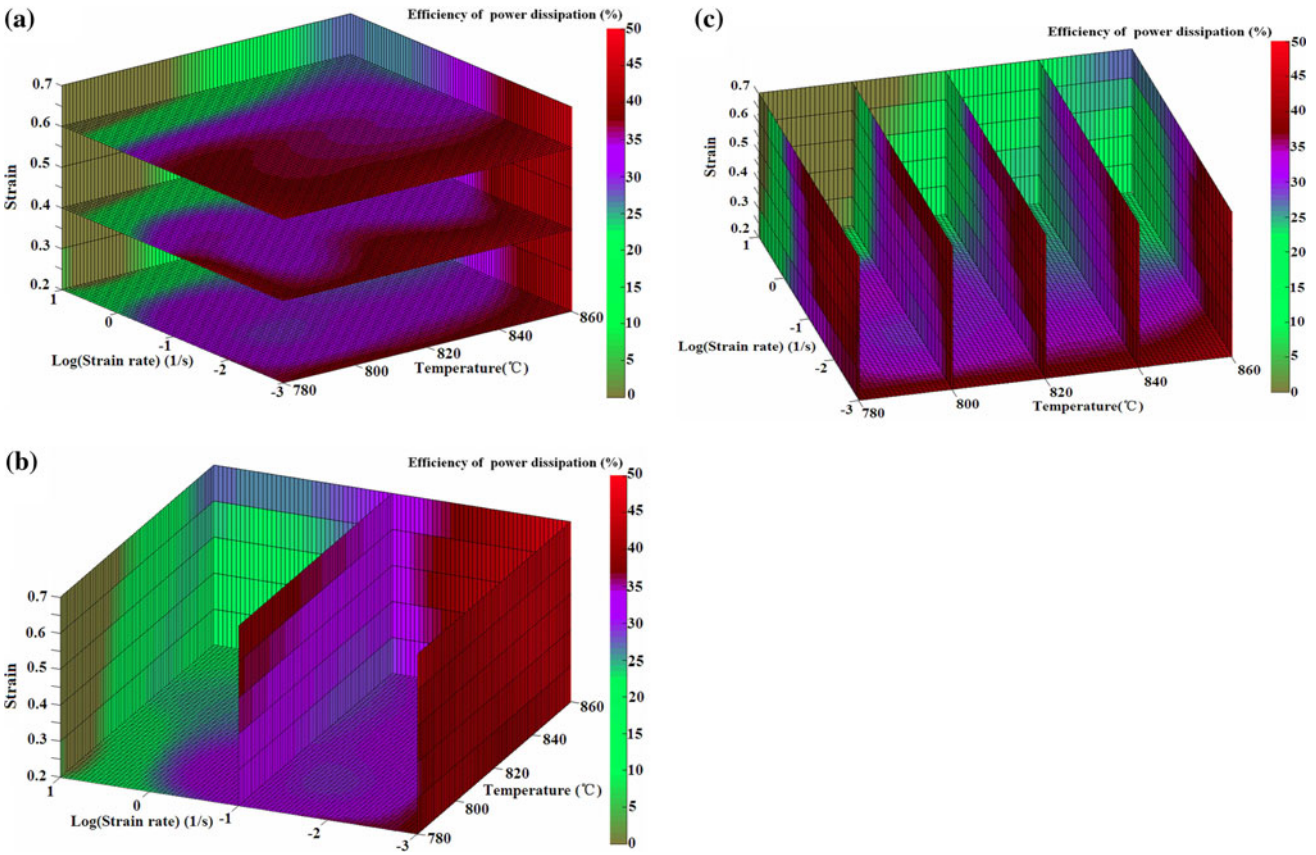

Fig. 4 3-D power dissipation maps **a** at different strains 0.2, 0.4, and 0.6, **b** at different strain rates 10, 0.1, and 0.001 s^{-1}, **c** at different temperatures 780, 800, 820, 840, and 860 °C

domains. The first domain of maximum power dissipation with a peak efficiency of 46% (at 860 °C and 0.001 s^{-1}) in the temperature range of 800–860 °C and at strain rate lower than 0.01 s^{-1}. A similar domain in higher temperatures and lower strain rates has been recorded by Seshacharyulu et al. [3] on commercial grade Ti–6Al–4V with starting lamellar structure and by Li et al. [7] on Ti–6Al–3Mo–2Zr–0.3Si, also with starting lamellar structure. Furthermore, there are other domains of maximum power dissipation with a peak efficiency of 41% (at 780 °C and 0.001 s^{-1}) in the temperature range of 780–800 °C and at strain rates lower than 0.01 s^{-1}. As titanium alloys are characterized by a high stacking fault energy, high values of power dissipation (>40%) are expected as soon as dynamic recrystallisation (globularization) [10] or superplasticity [22] occurs. Conventionally, superplasticity occurrence must possess three factors: one is equiaxed, finely grained, and stabilized microstructure, while the others are associated with testing under high temperature and low strain rate conditions. Moreover, the efficiency of power dissipation is generally very high (>60%) [13] and the strain rate sensitivity (m) is 0.6–0.9 [22] as soon as the superplastic deformation in titanium alloys occurs. But in two peak domains in the map the maximum efficiency is only about 46% and the strain rate sensitivity (m) is 0.24–0.26. Therefore, the interpretation of superplasticity would seem to be ruled out in two peak domains. The similar dissipation power domain has been interpreted in terms of DRX or dynamic globularization of lamellar structure in Ti–6Al–4V [3] and Ti–6Al–3Mo–2Zr–0.3Si [7]. The processing map also predicts a large domain of flow instability at strain rates higher than 0.487 s^{-1} over almost the entire test temperature range. This is because of the possible occurrence of adiabatic shear bands or localized plastic flow. Adiabatic shear banding is an important thermoviscoplastic instability mode observed in metals when processed at high strain rates [7]. These above predictions on microstructural evolution mechanisms are further validated by the microstructural observations on the deformed specimens.

3-D processing maps of the Ti-17 alloy

Interpretation of 3-D power dissipation map

The 3-D maps of power dissipation of Ti-17 alloy at different strains, temperatures, and strain rates are shown in Fig. 4. In the power dissipation maps, the color of grid denotes the value (shown as a percentage) of efficiency of power dissipation. According to 3-D power dissipation maps, the effect of the strain, temperature, and strain rate on the efficiency of power dissipation are illuminated. The efficiency of power dissipation obviously increases with increasing strain at higher temperatures and lower strain rates, especially at strain rate lower than 0.01 s^{-1} (Fig. 4a). Moreover, the efficiency of power dissipation decreases with increasing strain rate (Fig. 4b), and it increases with increasing temperature, especially in the temperature range of 820–860 °C (Fig. 4c). The 3-D maps of power dissipation also exhibits maximum power dissipation efficiency in the temperature range of 820–860 °C and at strain rate lower than 0.01 s^{-1}. On the basis of the deformation microstructural observation (Figs. 5, 6), it can be concluded that the degree of dynamic globularization of lamellae increases with increasing strains, increasing temperature, and decreasing strain rate.

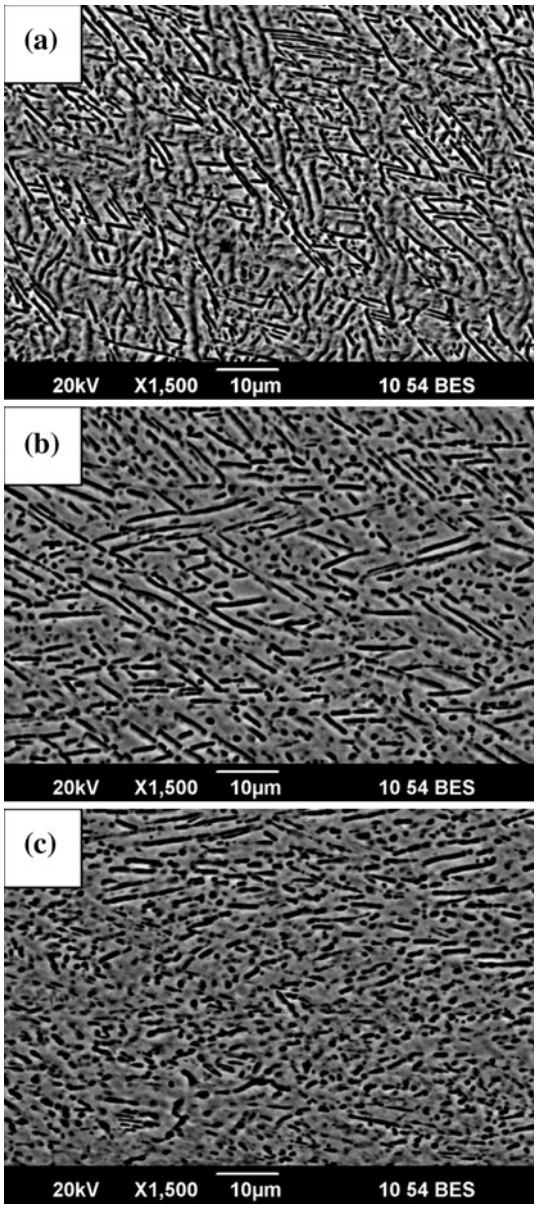

Fig. 5 SEM backscattered micrograph of Ti-17 alloy deformed at 860 °C and 0.001 s^{-1} under different strains of **a** 30%, **b** 45%, **c** 60%

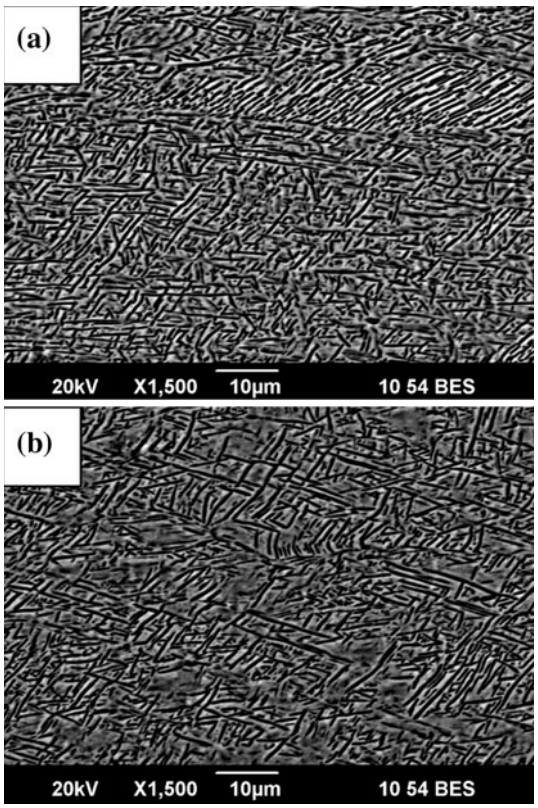

Fig. 6 SEM backscattered micrograph of Ti-17 alloy deformed at 820 °C, the strain of 45% and under different strain rates of **a** 0.001 s^{-1}, **b** 1 s^{-1}

Figure 5 shows the typical micrographs of globularization development of the lamellar structure at 860 °C and 0.001 s^{-1}, corresponding to a peak efficiency of power dissipation of about 46% in this domain (Figs. 3, 4). It is seen from SEM backscattered micrographs that the morphology of α phase is varied with strain significantly. At strain of 30% (Fig. 5a), a small amount of α lamellae broke up and slightly globularized, and there are about 20% (volume fraction) globularized α (Feret ratio $\leq$2.5 [23]). At strain of 45% (Fig. 5b), α lamellae broke up more remarkably and about 45% globularized α phase occurred. At strain of 60% (Fig. 5c), almost fully globularized (about 75%) or equiaxed microstructures with a small amount of broken-up alpha lamellae were readily observed. As the strain increases, the microstructures indicate significant morphological change of α phase from lamellar to globularized. Seshacharyulu et al. [6] regarded the dynamic globularization process as a type of DRX, but in the dynamic globularization process the nucleation of not new grains but interfaces in the lamellae appeared. The type of microstructural change involving a reduction in the aspect ratio of the lamellae can be interpreted in terms of geometric recrystallization [6, 7, 24]. Intense shear may fully sever α lamellae into two parts [25]. Other mechanisms of lamellae break-up is associated with the subboundary formation [25], which is easy to occur at the lamellar kinking. The globularization is induced by interface migration through the diffusion effect because of the driving force of lowering interfacial energy. Therefore, the globularization of α lamellae is strongly dependent on strain.

Figure 6 shows SEM backscattered micrographs of Ti-17 alloy deformed at different strain rates at 820 °C and the strain of 45%. It can be seen that the degree of dynamic globularization increases with the decreasing strain rate, and some kinking lamellae emerge at higher strain rates. This suggests that the globularization development of the lamellar structure is also dependent on strain rate. When the strain rate is relatively low (Fig. 6a), the dynamic globularization can proceed completely due to sufficient time for interface migration through the forceful diffusion effect. Fast deformation results in only a large number of lamellar kinking (in Fig. 6b), and little globularization due to insufficient time [7]. At higher strain rates, a number of part-separated lamellae can be observed through careful observation.

Comparing Fig. 5b with Fig. 6a, it can be concluded that the degree of the globularization noticeably increases with the increasing deformed temperature. With the

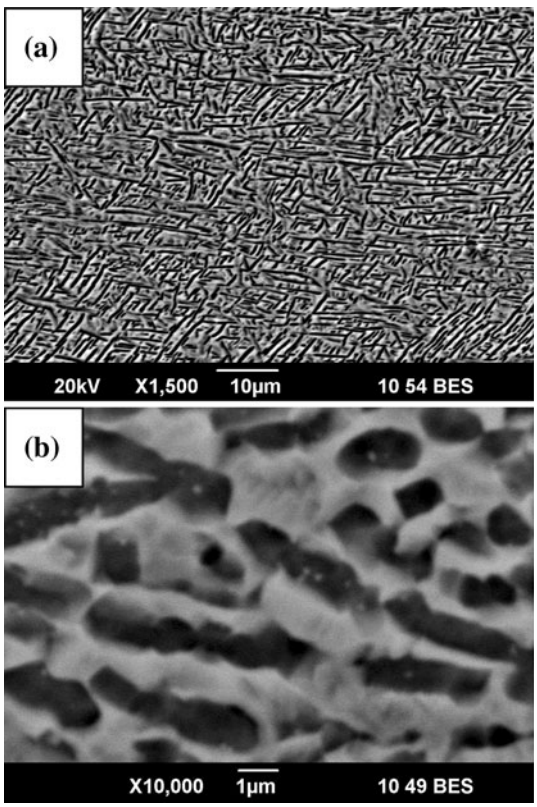

Fig. 7 SEM backscattered micrographs of Ti-17 alloy deformed at 780 °C, strain rate 0.001 s^{-1} and the strain of 60%

increasing of the temperatures, interfaces migration and lamellar termination migration due to powerful diffusional effect markedly accelerates the globularization process of α lamellae. This is because diffusion increases with the increase of temperature and thus dynamic globularization occurs more easily. The similar globularization characteristics under different strain rates and deformed temperature have been recorded in the Ti–6Al–4V alloy [3] and Ti–6Al–3Mo–2Zr–0.3Si [7].

There are other domains of maximum power dissipation in the range of lower temperatures (780–800 °C) at strain rates below 0.01 s^{-1}. Similar values of the efficiency of power dissipation and no instability imply that dynamic globularization should take place in this domain. Figure 7 shows SEM backscattered micrographs of Ti-17 alloy deformed at 780 °C and strain rate 0.001 s^{-1}. A number of short broken lamellae and coarse alpha lamellae with interface (subboundary) can be easily observed, but there are still low dynamic globularization fractions (about 22%) as a strain of 60%. It may be perhaps predicted that the element diffusion effect sharply decreases at the temperatures lower than 800 °C. At lower temperatures, the globularization process of lenticular α lamellae cannot be accomplished, because beta phase rarely penetrates into entire subboundaries through low diffusion. For short broken lamellae, it is also difficult to globularize through lamellar termination migration (driven by the urge to minimize the interfacial energy [26]). So the break-up or globularization of α lamellae in this domain is mainly associated with the localized shearing across α lamellae. An analysis on deformed microstructure and dynamic globularization kinetic of Ti-17 alloy has been detailedly established in our previous work [20, 27].

Interpretation of 3-D flow instability map

The 3-D maps of flow instability at different strains, temperatures, and strain rates are shown in Fig. 8. In the flow instability maps, the shadow color domain corresponds to flow instability of material. According to 3-D flow instability maps, an instability domain is located at strain rates higher than 0.487 s^{-1}, lower temperatures, and higher strain

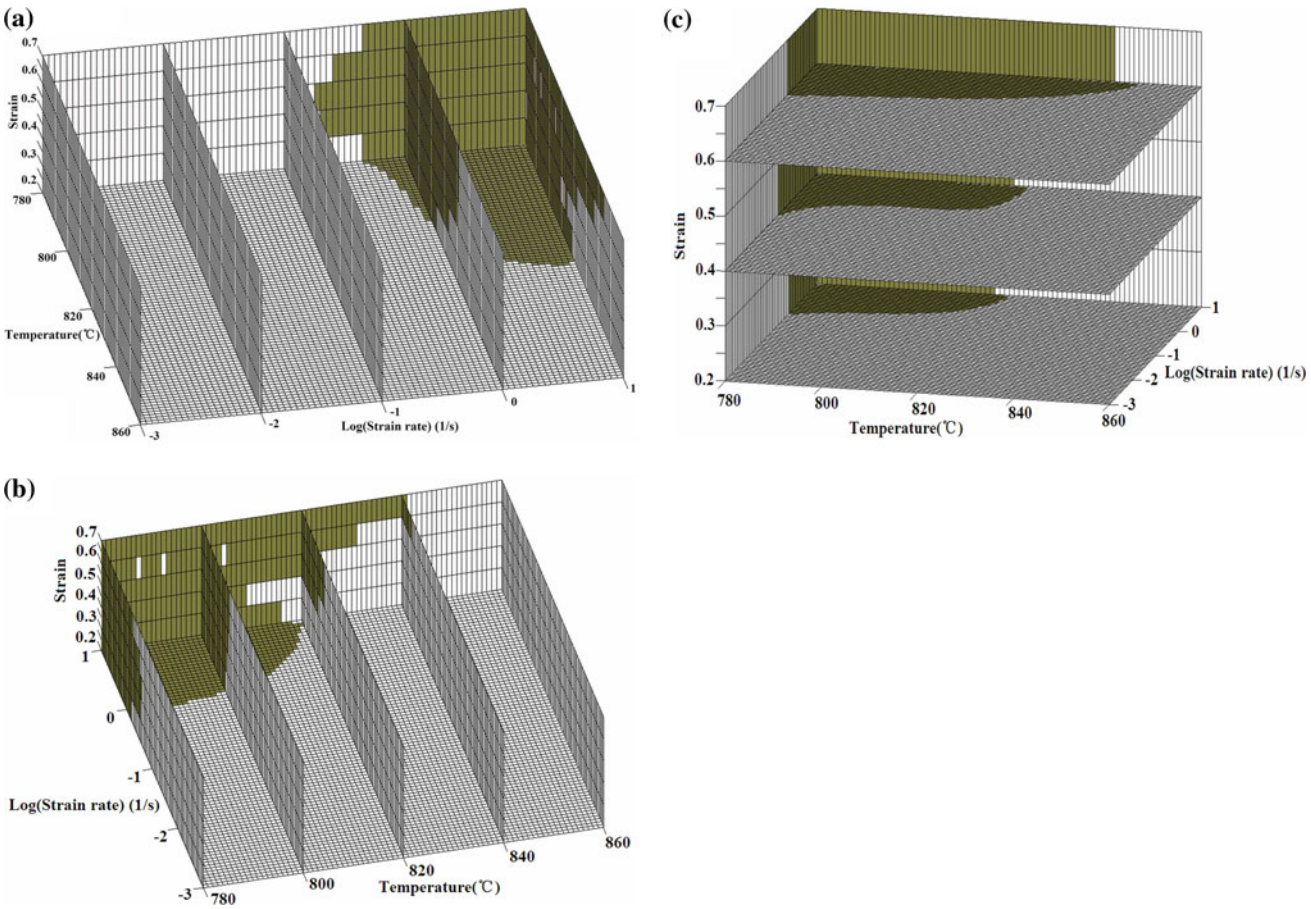

Fig. 8 3-D flow instability maps of Ti-17 alloy **a** at different strain rates 0.001, 0.01, 0.1, 1, and 10 s^{-1}, **b** at different temperatures 780, 800, 820, 840, and 860 °C, **c** at different strains 0.2, 0.4, and 0.6

above 0.2. The unstable deformation region increases with increasing strain, strain rate, and decreasing temperature. This has a good agreement with the oscillations of the stress–strain curves of Ti-17 alloys at higher strain rates. The microstructure of the specimen compressed at 780 °C and 10 s^{-1} exhibits adiabatic shear band at an angle 45° to the compression axis, as shown in Fig. 9. The formation of shear bands may be attributed to the adiabatic conditions created during deformation and the low thermal conductivity of Ti-17 alloy. At higher strain rates, adiabatic deformation heat is not conducted in short time so that highly localized flow appears along the maximum shear stress plane [7]. In Fig. 4, the low dissipation efficiency values may be seen in the domains corresponding to flow instability. This also suggests that most of the plastic power input converted to heat and was dissipated in the form of a temperature rise. Wang [28] suggested that the adiabatic shear band in TC16 alloy deformed at high strain rate ($>10^3 s^{-1}$) is the phase transformation band. However, the rapid heating effect at high strain rates has been recently employed to refine the grain due to accelerating the accumulation of defects in special deformation methods, for example hydrostatic extrusion [29]. In addition, lamellar kinking (Fig. 6b) at higher strain rates may result in flow instability [10]. Similar results are obtained in Ti–6Al–3Mo–2Zr–0.3Si [7], Ti600 alloy [8], and Ti–6Al–4V [3]. Therefore, the hot deformation of Ti-17 alloy should not be performed in this domain in order to avoid the generation deformation defects.

On the basis of above analysis, it is concluded that the optimum temperature can be selected from the temperature range of 800–860 °C and the optimum stain rate is 0.01 s^{-1} for obtaining the needed globularized microstructure in design of forging processes of Ti-17 alloy.

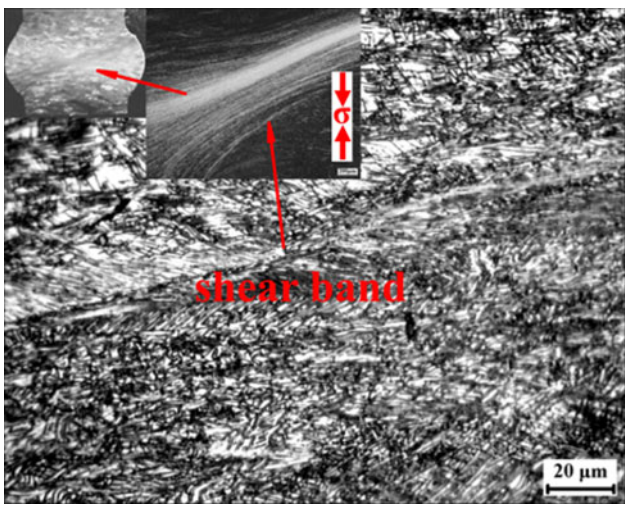

Fig. 9 Optical micrograph of Ti-17 alloy deformed at 780 °C, 10 s^{-1} and the strain of 30% showing adiabatic shear band

Conclusions

Hot deformation behavior of Ti-17 alloys with lamellar starting structure was characterized with the help of isothermal compression tests in the temperature range of 780–860 °C and strain rate range of 0.001–10 s^{-1}. On the basis of the traditional processing maps, 3-D processing maps including strain are developed and used to identify various microstructural mechanisms and distinguish the safe and unsafe domains. The following conclusions can be drawn from this investigation.

(1) The processing maps exhibit two maximum power dissipation efficiency domains: the one occurs at 800–860 °C and at strain rates lower than 0.01 s^{-1}, and the other occurs at 780–800 °C and at strain rates lower than 0.01 s^{-1}. With the increasing of the strains, the values of maximum power dissipation efficiency in two peak domains increase. Dynamic globularization of α lamellae takes place in these two domains, but in the latter domain the globularization process of α lamellae cannot successfully accomplish due to low diffusional effect.

(2) Flow instability occurs at strain rates higher than 0.487 s^{-1}, lower temperatures and strain above 0.2, which is induced by adiabatic shear bands and lamellar kinking. The instable deformation region increases with increasing strain, strain rate, and decreasing temperature.

(3) To obtain the required globularized microstructure in Ti-17 alloy, the optimum temperature can be selected from the temperature range of 800–860 °C and the optimum stain rate less than 0.01 s^{-1} in design of forging processes.

Acknowledgements The authors thank the financial supports from the State Key Foundational Research Plan (No.2007CB613807) and the Program for New Century Excellent Talents in University (NCET-07-0696).

References

1. Boyer R, Welsch G, Collings EW (eds) (1994) Materials properties handbook: titanium alloys. ASM International, Materials Park, OH, p 453
2. Tamirisakandala S, Vedam BV, Bhat RB (2003) J Mater Eng Perform 12:666
3. Seshacharyulu T, Medeiros SC, Frazier WG, Prasad YVRK (2002) Mater Sci Eng A 325:112
4. Prasad YVRK, Seshacharyulu T, Medeiros SC, Frazier WG (2001) J Mater Process Technol 108:320
5. Prasad YVRK, Seshacharyulu T (1998) Mater Sci Eng A 243:82
6. Seshacharyulu T, Medeiros SC, Morgan JT, Malas JC, Frazier WG, Prasad YVRK (2000) Mater Sci Eng A 279:289
7. Li AB, Huang LJ, Meng QY, Geng L, Cu XP (2009) Mater Des 30:1625

8. Niu Y, Hou H, Li M, Li Z (2008) Mater Sci Eng A 492:24
9. Jun Z, Weidong Z, Ying S, Yigang Z (2006) Rare Metal Mater Eng 35:265
10. Poletti C, Degischer HP, Kremmer S, Marketz W (1998) Mater Sci Eng A 486:127
11. Li X, Lu SQ, Fu MW, Wang KL, Dong XJ (2010) J Mater Process Technol 210:370
12. Liu J, Cui Z, Congxin L (2008) J Mater Process Technol 205:497
13. Prasad YVRK, Seshacharyulu T (1998) Int Mater Rev 43:243
14. Prasad YVRK (2003) J Mater Eng Perform 12:638
15. Prasad YVRK, Sasidhara S (1997) Hot working guide: a compendium of processing maps. ASM International, Materials Park, OH
16. Kalyan Kumar AKS (1987) MS Thesis, Indian Institute of Science, Bangalore, India, p 91
17. Zong YY, Shan DB, Lu Y (2006) J Mater Sci 41:3753. doi:10.1007/s10853-006-2658-z
18. Semenova IP, Valiev RZ, Yakushina EB, Salimgareeva GH, Lowe TC (2008) J Mater Sci 43:7354. doi:10.1007/s10853-008-2984-4
19. Chauhan VS, Misra A (2008) J Mater Sci 43:5634. doi:10.1007/s10853-008-2590-5
20. Wang KX, Zeng WD, Zhao YQ, Lai YJ, Zhang XM, Zhou YG (online press) Mater Sci Technol. doi:10.1179/174328409X463252
21. Seshacharyulu T, Medeiros SC, Frazier WG, Prasad YVRK (2000) Mater Sci Eng A 284:184
22. Sherby OD, Caiigiuri RD, Kayaii ES, White RA (1981) In: Burke JJ, Mahrabian R (eds) Advances in metal processing. Plenum Press, New York, p 133
23. Wang K, Zeng W, Shao Y, Yongqing Z, Yigang Z (2009) Rare Metal Mater Eng 38:398
24. Semiatin SL, Seetharaman V, Weiss I (1999) Mater Sci Eng A 263:257
25. Weiss I, Froes FH, Eylon D, Welsch GE (1986) Meter Trans A 17:1935
26. Stefasson N, Semiatin SL (2003) Meter Trans A 34:691
27. Wang K, Zeng W, Zhao Y, Lai Y, Zhou Y (2010) Mater Sci Eng A 527:2559
28. Wang BF (2008) J Mater Sci 43:1576. doi:10.1007/s10853-007-2330-2
29. Lewandowska M, Kurzydlowski KJ (2008) J Mater Sci 43:7299. doi:10.1007/s10853-008-2810-z